Earth and Planetary Science Letters 295 (2010) 1–11

Contents lists available at ScienceDirect

Earth and Planetary Science Letters

journal homepage: www.elsevier.com/locate/epsl

Non-nucleosynthetic heterogeneity in non-radiogenic stable Hf isotopes: Implications for early solar system chronology

Peter Sprung [a,c,*], Erik E. Scherer [a], Dewashish Upadhyay [a,d], Ingo Leya [b], Klaus Mezger [a,e]

[a] Institut für Mineralogie, WWU Münster, Corrensstrasse 24, 48149 Münster, Germany
[b] Physikalisches Institut, Universität Bern, Sidlerstrasse 5, 3012 Berne, Switzerland
[c] Institut für Geochemie und Petrologie, ETH Zürich, NW C 81.2, Clausiusstrasse 25, 8092 Zürich, Switzerland
[d] Department of Geology and Geophysics, Indian Institute of Technology, Kharagpur, 721302 Kharagpur, India
[e] Institut für Geologie, Universität Bern, Baltzerstrasse 1+3, 3012 Bern, Switzerland

ARTICLE INFO

Article history:
Received 9 September 2009
Received in revised form 22 February 2010
Accepted 26 February 2010
Available online 14 April 2010

Editor: R.W. Carlson

Keywords:
non-radiogenic stable Hf isotopes
nucleosynthesis
secondary neutron capture
Lu–Hf
CHUR
early Earth

ABSTRACT

Nucleosynthetic heterogeneity and secondary neutron capture reactions may have important implications for ^{176}Lu–^{176}Hf chronology and modelling of early planetary evolution. So far, the relevance of these phenomena for the Lu–Hf system has not been explored. We therefore have analyzed the non-radiogenic stable Hf-isotope composition (^{177}Hf, ^{178}Hf, ^{179}Hf, and ^{180}Hf) of meteorites, meteorite components, and terrestrial rock samples to identify nucleosynthetic or neutron capture-induced variations. All analyzed chondrites have uniform ^{178}Hf/^{177}Hf and ^{180}Hf/^{177}Hf values that cannot be resolved from the average terrestrial composition. Thus, there is no evidence for nucleosynthetic heterogeneity in chondrites or Earth and these data support the use of a chondritic reference value for the Hf-isotope composition of the Bulk Silicate Earth. This homogeneity contrasts with nucleosynthetic heterogeneities found in lighter elements and provides evidence for a separate synthesis of light and heavy r-process nuclei.
Various mesosiderite samples and one lunar meteorite display coupled ^{178}Hf/^{177}Hf and ^{180}Hf/^{177}Hf anomalies that are associated with neutron capture-induced deviations in ^{149}Sm/^{154}Sm and ^{150}Sm/^{154}Sm. However, the analyzed chondrites and an aubrite show only Sm-isotope anomalies, and these are the result of neutron capture. The Hf-isotope anomalies require substantial capture of epithermal neutrons, whereas Sm anomalies result primarily from thermal neutron capture. The non-radiogenic stable isotope composition of Hf is thus a suitable monitor for epithermal neutron capture reactions. The data reveal distinct neutron energy spectra: mesosiderites are characterized by high epithermal-to-thermal neutron fluence ratios, whereas the remaining samples show low epithermal-to-thermal ratios.
Secondary neutron capture may significantly increase the measured ^{176}Hf/^{177}Hf in whole-rock meteorite samples without causing a resolvable shift in ^{176}Lu/^{177}Hf. Thus it could potentially induce scatter in Lu–Hf whole-rock isochrons and produce spurious initial ^{176}Hf/^{177}Hf values. However, the slopes of internal (i.e., mineral) isochrons cannot be increased significantly by secondary neutron capture. This process therefore cannot account for the unrealistically old ^{176}Lu–^{176}Hf 'ages' (e.g., ~4.75 Ga) of some meteorites.

1. Introduction

The long-lived ^{176}Lu–^{176}Hf decay system provides a powerful geochronometer and isotopic tracer for geochemical modelling (e.g., Patchett, 1983). When applied to Archean rocks and minerals, it can be used to reconstruct timing and degree of large-scale silicate differentiation events early in Earths' history (e.g., Vervoort et al., 1996; Amelin et al., 1999). The system, however, can only be fully utilized if the bulk Lu/Hf and the initial ^{176}Hf/^{177}Hf of the planetary body in question and the ^{176}Lu decay constant are well constrained.

Being refractory and lithophile elements, Lu and Hf are assumed not to have been fractionated significantly from each other during processes of nebular evaporation, condensation, or planetary core formation. This assumption is supported by the tightly defined chondritic Lu/Hf value of Bouvier et al. (2008). Thus, the solar composition and also that of the bulk silicate portion of terrestrial planetary bodies are taken to have a chondritic Lu/Hf (e.g., Palme and Jones, 2007). Different classes and petrologic types of chondrites form a correlated array in ^{176}Hf/^{177}Hf vs. ^{176}Lu/^{177}Hf space (e.g., Blichert-Toft and Albarède, 1997). A chondritic reference value for the Lu–Hf system has been defined as the ^{176}Hf/^{177}Hf

* Corresponding author. Institut für Geochemie und Petrologie, ETH Zürich, NW C 81.2, Clausiusstrasse 25, 8092 Zürich, Switzerland. Tel.: +41 44 632 35 62; fax: +41 44 632 11 79.
E-mail addresses: sprungp@uni-muenster.de, peter.sprung@erdw.ethz.ch (P. Sprung), escherer@uni-muenster.de (E.E. Scherer), upadhyay@uni-muenster.de, dewashish@gg.iitkgp.ernet.in (D. Upadhyay), ingo.leya@space.unibe.ch (I. Leya), klaus.mezger@geo.unibe.ch (K. Mezger).

0012-821X
doi:10.1016/j.epsl.2010.02.050

value of this array at its mean $^{176}Lu/^{177}Hf$ (Blichert-Toft and Albarède, 1997). Using an alternative approach, Patchett et al. (2004) concluded by comparing combined Lu–Hf and Sm–Nd data of chondrites and terrestrial samples that the mean of carbonaceous chondrites might represent a plausible alternative reference value for the Bulk Silicate Earth (BSE). Most recently, Bouvier et al. (2008) improved upon earlier studies by analyzing unequilibrated chondrites (types 1–3, mostly falls), thereby significantly reducing the spreads in Lu/Hf and $^{176}Hf/^{177}Hf$, and the uncertainties on their mean values. However the possibilities of 1) initial nucleosynthetic Hf-isotope heterogeneity or 2) secondary nuclear effects have not yet been thoroughly investigated. A uniform initial $^{176}Hf/^{177}Hf$ of the solar system requires that the Hf nuclides were homogeneously distributed in the solar nebula. To determine this initial value, the effects of secondary processes such as radiogenic ingrowth, secondary chemical fractionation, and nuclear reactions must be identified and accurately quantified. Here we evaluate the possible extent of nucleosynthetic heterogeneities and secondary nuclear effects by analyzing the non-radiogenic stable Hf-isotope composition of meteorites, meteorite components, and terrestrial rocks. The importance of such a study is highlighted by recent findings of isotope anomalies in *bulk* meteorite samples for elements such as Ba, Cr, Fe, Nd, Mo, Ni, Sm, and Ti (e.g., Rotaru et al., 1992; Yin et al., 2002; Hidaka et al., 2003; Bizzarro et al., 2007; Carlson et al., 2007; Quitté et al., 2007; Leya et al., 2008a; Regelous et al., 2008), which indicate that initial nucleosynthetic heterogeneities have been preserved.

Hafnium isotopes are produced in a variety of nucleosynthetic processes. The neutron-deficient ^{174}Hf isotope and possibly ~3% of ^{176}Hf (Klay et al., 1991) were produced by the p-process, which has been attributed to environments such as supernovae or massive stars in their pre-supernova phase (Arnould and Goriely, 2003). The majority of ^{176}Hf, however, is of s-process origin. In contrast, ^{177}Hf, ^{178}Hf, ^{179}Hf, ^{180}Hf, and ^{182}Hf had contributions from both s- and r-process (Wisshak et al., 2006; Vockenhuber et al., 2007). The s-process is commonly attributed to thermally pulsing, low-mass, asymptotic giant branch (AGB) stars (Busso et al., 1999). The r-process is thought to comprise different rapid neutron capture processes that occur in various stellar environments such as supernovae or neutron star mergers. The common characteristic of these processes is a high neutron density, which is possible in various temperature regimes (e.g., Meyer and Adams, 2006; Arnould et al., 2007). Further nuclear reactions, including charged particle reactions, can contribute to the r-process synthesis of lighter nuclei ($\sim Z \leq 56$; e.g., Qian and Wasserburg, 2007).

Quantifying radiogenic ^{176}Hf ingrowth requires that the decay constant of ^{176}Lu is accurately and precisely known. There is however an unsolved discrepancy between ^{176}Lu decay constant determinations based on meteorites (e.g., Patchett and Tatsumoto, 1980; Bizzarro et al., 2003) and those based on terrestrial samples (Scherer et al., 2001, 2003; Söderlund et al., 2004). Possible explanations for the apparently accelerated decay of ^{176}Lu in meteorites include the excitation of ^{176}Lu via γ-irradiation (Albarède et al., 2006) or interactions with ultra-relativistic cosmic-rays or neutrinos (Thrane et al., 2006; Meyer et al., 2008). Given the good agreement among ^{176}Lu decay constant calibrations that are based on terrestrial samples, the application of the ^{176}Lu decay constant to terrestrial data sets appears to be justified (Söderlund et al., 2004). Yet, the discrepancy is still the subject of ongoing research.

One particularly important nuclear effect that has long been known to significantly modify primary isotope compositions is the capture of secondary neutrons (n-capture) by nuclides having large n-capture cross sections (e.g., Lingenfelter et al., 1972; Leya et al., 2000). Highly energetic galactic cosmic-rays (~0.1 to ~10 GeV) interact with matter and produce fast to moderately fast secondary neutrons. These are moderated to epithermal (~0.025 eV to a few keV) and thermal (~0.025 eV at room temperature) energies by elastic scattering and other nuclear reactions (e.g., Lingenfelter et al., 1972; Gosse and Phillips, 2001). The resulting neutron energy spectrum depends on the size and chemical compositions of the target body and the depth within the target (e.g., Leya, 1997; Kollár et al., 2006). In particular, H, O, Si and Fe contents have a strong influence on the moderation of neutrons to thermal energies and thus on the relative magnitudes of thermal and epithermal neutron fluences (Lingenfelter et al., 1972; Kollár et al., 2006). Capture of epithermal and thermal neutrons by nuclei changes the isotope abundances of the target material. The average probability for capturing a neutron (cross section) scales with the inverse of the neutron velocity (i.e. capture probability $\sim 1/v$). Superimposed on this dependence are discrete energies at which the n-capture probability is enhanced, the so-called resonances. For thermal neutrons, the $1/v$ dependence usually is sufficient for predicting capture rates, and thus the thermal neutron capture cross sections are defined. In the epithermal region, however, resonances are important for defining the epithermal analogue to the thermal cross section, the resonance integral (RI). The destruction (i.e., burnout) and production of isotopes important to the Lu–Hf system depend on the energy spectrum of the secondary neutrons and the integrated neutron flux (n/cm²). At *epithermal* energies, the most probable reactions are n-capture on ^{177}Hf and ^{178}Hf, i.e., $^{177}Hf(n,\gamma)^{178}Hf$ (RI of ~7210 barn) and $^{178}Hf(n,\gamma)^{179}Hf$ (RI of ~1910 barn), respectively. These affect all ^{177}Hf-referenced Hf-isotope ratios directly via changing the ^{177}Hf abundance and indirectly by increasing $^{179}Hf/^{177}Hf$, which is commonly used for mass-bias correction. Because all Hf-isotope abundances are modified, such n-capture effects cannot be avoided by using a different normalizing ratio. At *thermal* energies, the most probable n-capture reaction is the transformation of ^{176}Lu to ^{177}Hf, i.e., $^{176}Lu(n,\gamma)^{177}Lu \rightarrow {}^{177}Hf + e^- + \bar{\nu}$, with a thermal n-capture cross section (σ_{th300K}) of ~3640 barn. Another sensitive monitor of secondary n-capture reactions is the transformation of ^{149}Sm to ^{150}Sm (e.g., Lingenfelter et al., 1972; Nyquist et al., 1995; Hidaka et al., 2000): ^{149}Sm has a large capture cross section for both thermal and epithermal neutrons (σ_{th300K} ~70,040 barn and RI of ~3480 barn). Here, using measurements of non-radiogenic stable Sm- and Hf-isotope compositions, the first findings of neutron-capture-induced changes of Hf-isotope abundances in meteorites are reported. The implications for geochemical modelling and for ^{176}Lu–^{176}Hf chronology are discussed.

2. Sample description and analytical techniques

A variety of terrestrial and extra-terrestrial rock samples were selected for this study. The terrestrial samples comprise Archean to Quaternary igneous and metamorphic rocks ($n = 20$), including four international rock standards (AGV-2, BCR-2, BHVO-2, and JG-2). This selection was made to test for potential temporal variations in the non-radiogenic stable Hf-isotope compositions in terrestrial rocks. The extra-terrestrial samples include chondrites, mesosiderites, one lunar meteorite (DAG 262), one aubrite (Peña Blanca Springs), three dark inclusions (two from NWA 753, one from Allende), and two Ca–Al-rich inclusions (CAI) from Allende. The chondrite suite includes four carbonaceous chondrites (Allende — CV3, Dar al Gani 275 — CK4/5, Dar al Gani 137 — CO3, and Murchison — CM2), eight ordinary chondrites (Dar al Gani 318 — H3, Acfer 105 — H4, El Hammami — H5, Acfer 111 — H3-6, Dar al Gani 216 — L3, Acfer 029 — L6, Dar al Gani 301 — L6, and Acfer 066 — LL3-6), and one Rumuruti chondrite (NWA 753 — R3.9). The chondritic regolith breccias Acfer 066 and Acfer 111 were chosen because of their known regolith irradiation histories and high solar noble gas contents (Pedroni and Begemann, 1994; Jäckel et al., 1997; Scherer et al., 1998). The mesosiderite samples comprise five 'basaltic' pebbles, two pyroxene fractions from two 'basaltic' pebbles, and one 'gabbroic' pebble (see classification of Rubin and Mittlefehldt, 1992) from Vaca Muerta (hereafter VM), as well as silicate inclusions from Estherville and Mincy.

Table 1
Two-stage Hf separation scheme and Lu-cleanup chemistry using ion-exchange chromatography on Eichrom® Ln-Spec resin. At loading volumes greater than 20 ml, 2 M HCl instead of 3 M HCl is used to improve Lu yields. The Ti-separation step uses the acid volume necessary to achieve a colourless eluate and then another 10 additional ml of the same acid are added. For ID-only analyses the Zr-separation step is omitted from the Hf-cleanup (stage 2). One 'reservoir' refers to the acid volume filling the whole column.

(1–1.2 ml Eichrom® Ln-spec resin 100–200 mesh; resin bed length: 3.8 cm)		
Stage 1: separation of Lu and Hf from matrix		
Step	Volume, ml	Reagent
Equilibrate resin	2×5	2–3 M HCl
Load sample, collect matrix + LREE	10–70	2–3 M HCl
Rinse, collect matrix + LREE	10	3 M HCl
Collect Lu + some Yb	12	6 M HCl
Rinse remaining Lu off column	2×10	6 M HCl
Rinse column	2×2	H_2O
Rinse Ti off column	2–10×10	0.45 M HNO_3–0.09 M citric acid–1 vol.% H_2O_2
Rinse column	2×2	H_2O
Rinse Zr off column	5×10	6 M HCl–0.06 M HF
Collect Hf	12	2 M HF
Clean	1 reservoir	6 M HCl
Clean	1 reservoir	2 M HF
Clean	2	H_2O
Stage 2: Hf-cleanup (same column as above)		
Equilibrate resin	2×5	3 M HCl
Load Fe-bearing Hf sample	10	3 M HCl–0.1 M ascorbic acid
Rinse Fe off column	10	3 M HCl
Rinse remaining HREE off column	1–2×10	6 M HCl
Rinse Zr off column (for ICs only)	4×10	6 M HCl–0.06 M HF
Collect Hf	12	2 M HF
Clean	1 reservoir	6 M HCl
Lu-cleanup (same column as above)		
Equilibrate resin	2×5	1 M HCl
Load Fe-bearing Lu sample	5–10	1 M HCl–0.1 M ascorbic acid
Rinse Fe off column	10	1 M HCl
Collect Lu	12	6 M HCl
Clean	1 reservoir	6 M HCl
Clean	1 reservoir	2 M HF
Clean	1 reservoir	6 M HCl

Details concerning sample preparation, digestion techniques, and chemical separation of Hf, Lu, and Sm are given in the Supplementary data. The Hf separation by ion-exchange chromatography (Table 1) is based on established methods that use Eichrom® Ln-Spec resin (Münker et al., 2001; Weyer et al., 2002). For five of the VM pebbles, the two VM pyroxene fractions, eight chondrites, the lunar meteorite, and the aubrite, Sm was separated from the bulk matrix fraction of the first stage Ln-Spec column.

Initially, Hf was analyzed in static mode on the Micromass Isoprobe MC-ICP-MS at Münster using the collector configuration and baseline measurement scheme described in Münker et al. (2001). Later, improved reproducibility for $^{176}Hf/^{177}Hf$ measurements was achieved by using the on-peak-zero method, whereby baselines were measured on a solution blank for 50 s before each analysis. Mass bias was corrected using two different methods: 1) An empirical, $^{179}Hf/^{177}Hf$-normalized scheme derived from the considerations of Maréchal et al. (1999) regarding the general properties of mass bias in plasma-source mass spectrometers, and 2) according to the exponential law as described by Russel et al. (1978) and normalized to $^{179}Hf/^{177}Hf$. The empirical normalizing scheme was applied for sessions during which the magnitude of the mass bias varied strongly: Within an analytical session, interference-corrected (but not mass-bias corrected) isotope ratios from multiple analyses of isotopically identical standard solutions display a linear relationship in $\ln(^{1xx}Hf/^{177}Hf)$ vs. $\ln(^{179}Hf/^{177}Hf)$ space. Mass-bias-corrected isotope compositions of samples are then calculated as the ppm difference between the measured $^{1xx}Hf/^{177}Hf$ of the sample and that of the linear standard trend at the sample's measured $^{179}Hf/^{177}Hf$. The Hf standard solution was prepared from an Ames Hf metal ingot and is isotopically indistinguishable from the JMC-475 standard, whose composition is taken to be $^{178}Hf/^{177}Hf = 1.46717$ and $^{180}Hf/^{177}Hf = 1.8868$ at $^{179}Hf/^{177}Hf = 0.7325$ (Scherer et al., 2000). Interleaving analyses of standards and samples enabled the correction of instrumental drift. Analyzing standard solutions that had concentrations bracketing those of the sample solutions enabled the correction of analytical bias related to signal strength. Thirty-five solution replicates of one terrestrial basanite digestion (NZ 557, Sprung et al., 2007) over the course of the study yielded a 2σ (=2 SD) reproducibility of 19 ppm for $^{178}Hf/^{177}Hf$ and 34 ppm for $^{180}Hf/^{177}Hf$ (using 40–60 ng Hf per analysis). This compares well with the external reproducibility of all standard analyses in which a similar amount of Hf was consumed (14 ppm for $^{178}Hf/^{177}Hf$ and 36 ppm for $^{180}Hf/^{177}Hf$; $n = 264$). All results were normalized such that the session average of all standard analyses equalled the assumed standard composition. The external 2 SD reproducibilities of single sample analyses ($2\sigma_{sample}$, Table S1) was estimated from the relationship between the 2 SE internal run statistics and the 2 SD external reproducibility of standards that were analyzed during the same session (Bizzarro et al., 2003; Table S2, this study). For sessions in which the number

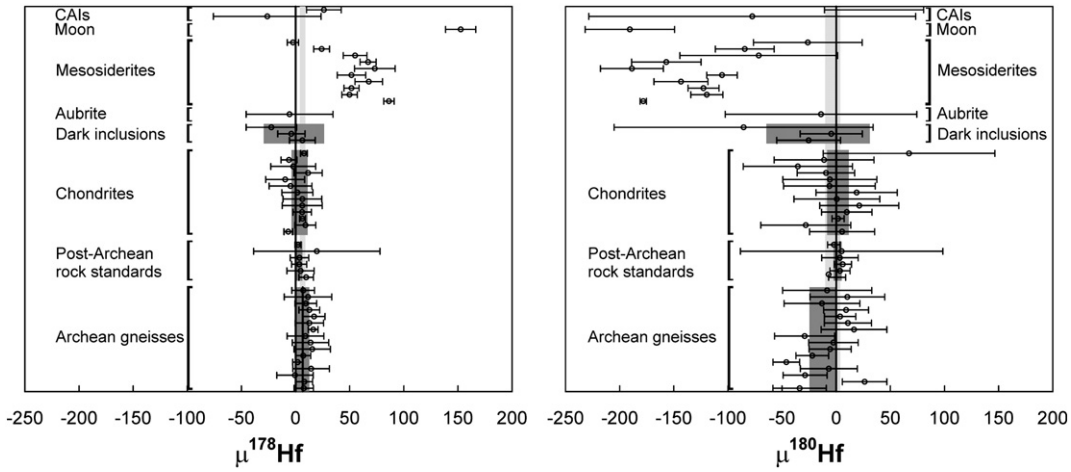

Fig. 1. $\mu^{178}Hf$ (left panel) and $\mu^{180}Hf$ (right panel) of all analyzed samples. Details concerning mass-bias corrections (normalizing to $^{179}Hf/^{177}Hf$) and the calculation of μ-values are described in Section 2. Individual error bars are $2\sigma_\mu$. The solution standard composition is given by the bold vertical lines at 0; grey boxes: 95% confidence limits of population means; light grey vertical bars: 95% confidence limits of the weighted mean of all terrestrial samples; CAI 2 (uppermost sample) is shown with 95% confidence limits; samples on each panel from bottom to top are in the same order as in Table 2.

of standard analyses at different concentrations was insufficient for the application of this procedure, the analogous relationships displayed by all standard analyses of the whole project were used. We report $^{178}Hf/^{177}Hf$ and $^{180}Hf/^{177}Hf$ data as deviations in ppm (μ-values) from the average value of all standard analyses measured during the same analytical session ($\mu^{1xx}Hf = \{[^{1xx}Hf/^{177}Hf]_{sample}/[^{1xx}Hf/^{177}Hf]_{avg.\ std.} - 1\} \times 10^6$). For inter-session comparison of μ-values and to better visualize anomalies resolved from the solution standard, a combined uncertainty ($2\sigma_\mu$) was defined, incorporating the 2 SE uncertainty of all standard analyses during the same session ($2\sigma_{m\ avg.\ std.}$) and the estimated 2 SD ($2\sigma_{sample}$) external reproducibility for each sample ($2\sigma_\mu = \sqrt{(2\sigma_{sample})^2 + (2\sigma_{m\,avg.std.})^2}$). Solution replicates as well as digestion replicates were pooled to give weighted averages with their associated 2 SE uncertainties (Fig. 1). For small numbers of replicates, this uncertainty does *not* imply 95% confidence. For population means (Archean gneisses, chondrites, and international rock standards), we report the weighted mean with 95% confidence limits.

Samarium isotopes were measured in static mode on a Finnigan Triton thermal ionization mass spectrometer (TIMS) using double Re-filaments. Mass fractionation was corrected with the exponential law and a $^{147}Sm/^{154}Sm$ of 0.65918 (Rankenburg et al., 2006). Isobaric interferences from Nd and Gd on Sm masses were corrected by monitoring interference-free masses of the respective elements and subtracting the contributions of ^{152}Gd, ^{154}Gd, ^{144}Nd, ^{148}Nd, and ^{150}Nd from the respective total signals on each mass. For some samples (Table S3), La-oxide signals (identified by background scans) on the ^{155}Gd interference monitor caused an overcorrection for Gd-interferences. Not applying a Gd interference correction for these samples improved the coherency of the Sm-isotope data set and moved the affected data points onto the n-capture trend defined by the remaining samples and the in-house Sm standard (Fig. 2). As with Hf, $\mu^{1xx}Sm$ values were calculated as ppm deviations from the average of all Sm standards analyzed during this study (Table S4).

For TIMS Sm data, the $2\sigma_\mu$ uncertainty is defined as the quadratic sum of the external 2 SD reproducibility of a sample (estimated to be equal to the external 2 SD of all analyzed Sm solution standards) and the external 2 SE reproducibility of all analyzed Sm standards (Table S4). In principle, this may underestimate the true sample uncertainties if samples were analyzed under different conditions than standards (i.e., lower signal intensities, shorter analysis time, variable matrix composition). However, an MSWD of ~1 together with the very good match of the n-capture trend defined by the samples and the in-house Sm standard (Fig. 2) to theoretical predictions for such a trajectory (i.e., slope = −1) appears to justify the chosen approach.

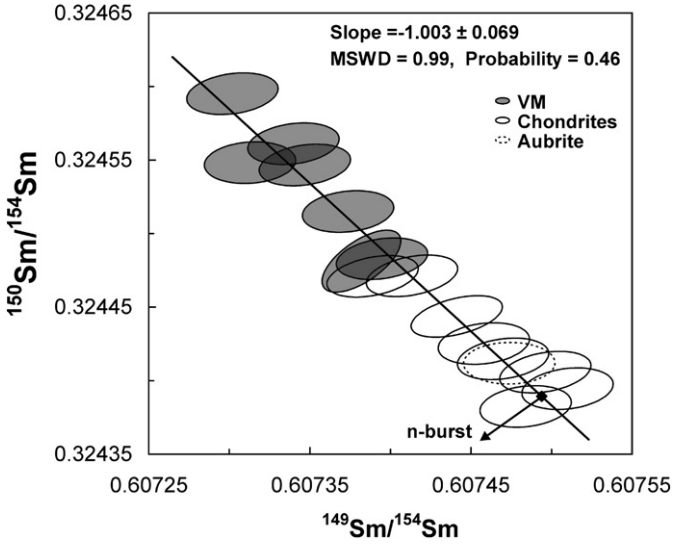

Fig. 2. Correlated deviation in $^{147}Sm/^{154}Sm$-normalized $^{149}Sm/^{154}Sm$ and $^{150}Sm/^{154}Sm$ of chondrites, VM and Peña Blanca Springs (Aubrite) due to secondary n-capture. The error ellipses depict $2\sigma_\mu$ uncertainties. The bold black line is a regression line through all data points and the standard composition which is given by the black diamond. Mixing of 'normal' Sm with n-burst Sm is illustrated by the arrow.

3. Results

3.1. Chondrites, dark inclusions, Peña Blanca Springs, CAIs, and terrestrial rocks

The 13 analyzed chondrites form a homogeneous group with $\mu^{178}Hf$ (+4 ± 7 ppm) and $\mu^{180}Hf$ (+2 ± 10 ppm) population means that are indistinguishable from the Münster Hf standard solution (Fig. 1). Unless noted otherwise, the quoted uncertainties of weighted averages are 95% confidence limits. Digestion replicates of three samples agree within their estimated uncertainties (Table 2, Table S1, Fig. 1). The dark inclusion data (population mean $\mu^{178}Hf = -1 \pm 28$ ppm and $\mu^{180}Hf = -17 \pm 48$ ppm, $n = 3$) and the data for Peña Blanca Springs ($\mu^{178}Hf = -6 \pm 40$ ppm and $\mu^{180}Hf = -14 \pm 88$ ppm) agree with the composition of the Hf standard solution. The compact, presumably type B CAI 2 yields weighted average $\mu^{178}Hf = +26 \pm 16$ ppm and $\mu^{180}Hf = +35 \pm 46$ ppm, respectively (95% confidence, $n = 3$). The other CAI (CAI 4, fluffy, presumably type A) overlaps the standard's composition. Combining all 20 terrestrial rock samples yields weighted means for $\mu^{178}Hf$ and $\mu^{180}Hf$ of +7 ± 3 ppm and −3 ± 7 ppm, respectively. The combined post-Archean rock samples have weighted mean $\mu^{178}Hf$ and $\mu^{180}Hf$ values of +3 ± 3 ppm and +1 ± 4 ppm, respectively. For the Archean gneisses, the average $\mu^{180}Hf$ is −12 ± 12 ppm. The measured $\mu^{178}Hf$ values for Archean gneisses (10 ± 3 ppm) are systematically higher than the standard values. Samarium-isotope compositions were obtained from Allende, Acfer 105, Acfer 066, Dar al Gani 216, Dar al Gani 318, Murchison, NWA 753, and Peña Blanca Springs (Table S3; Figs. 2 and 4). For El Hammami, the Sm-isotope data are from Upadhyay and Mezger (2008) and were measured on a different digestion than that used for the Hf analyses. Five of these chondrites and Peña Blanca Springs have resolved ^{149}Sm and ^{150}Sm anomalies of up to −173 ± 39 ppm and +253 ± 37 ppm, respectively.

3.2. Mesosiderites, Dar al Gani 262 (DAG 262)

Independent of their petrographic classification, all VM samples and the Estherville sample yield positive $\mu^{178}Hf$ values (up to +86 ± 5 ppm) that correlate negatively with $\mu^{180}Hf$ (as low as −189 ± 29 ppm; Table 2, Table S1, Fig. 3). The μ-values are well resolved from the standard composition and the weighted means of the other samples. (Fig. 1; Fig. 3). The VM samples also display negative $\mu^{149}Sm$ values (as low as −316 ± 39 ppm) that correlate negatively with $\mu^{150}Sm$ (up to +634 ± 37 ppm; Fig. 2).

Whereas $\mu^{178}Hf$ values show a negative correlation with $\mu^{149}Sm$ (Fig. 4), the $\mu^{180}Hf$ values display a positive correlation with $\mu^{149}Sm$ (not shown). Of the analyzed mesosiderite samples, only the Hf composition of Mincy agrees with that of the Hf standard solution. The lunar meteorite DAG 262 shows the largest anomalies both in Hf ($\mu^{178}Hf = +153 \pm 14$ ppm and $\mu^{180}Hf = -191 \pm 41$ ppm; Fig. 3) and in Sm ($\mu^{149}Sm$ as low as −5443 ± 39 ppm and $\mu^{150}Sm$ up to +10,122 ± 37 ppm) isotope composition. Positive $\mu^{152}Sm$ anomalies (Table S3) are observed only for the gabbroic VM pebble (+718 ± 24 ppm) and DAG 262 (+339 ± 24 ppm and +386 ± 24 ppm).

4. Discussion

4.1. No resolvable nucleosynthetic heterogeneity in chondrites, Earth, Peña Blanca Springs, and dark inclusions

The population means of $\mu^{178}Hf$ and $\mu^{180}Hf$ for chondrites, terrestrial rocks, Peña Blanca Springs, and the dark inclusions overlap. This implies

Table 2
Sample μ^{178}Hf and μ^{180}Hf values. Details concerning mass-bias corrections and the calculation of μ-values are described in Section 2. Abbreviations for sample groups: I: Post-Archean igneous rock standards; A: Archean Gneisses; C: Chondrites; DI: Dark inclusions; MS: Mesosiderites; CAI: Ca–Al-rich inclusions. The number of pooled analyses, including digestion replicates, is given by *n*. For sample CAI 2, 95% confidence limits are given in parentheses. For details on SE-3, see Schuth et al. (2004, 2009). References for cosmic-ray exposure (CRE): [1]weighted average of values given in Eugster et al. (2007); [2]Scherer and Schultz 2000; [3]assuming sample is part of the CO chondrite strewn field described in Schlüter et al. (2002); [4]Scherer et al. (1998); [5]Schultz et al. (2005); [6]Ebisawa et al. (2003); [7]individual chondrules: Roth et al. (2009); [8]Pedroni and Begemann (1994); [9]Lorenzetti et al. (2003); [10]Miura et al. (2007); [11]Begemann et al. (1976); [12]Nagao and Bajo (2006); [13]Schaeffer and Heymann (1965); [14]Albrecht et al. (2000); [15]Fernandes et al. (2000); [16]Eugster et al. (2000). Note that there is no simple linear relation between CRE ages and observed μ^{1xx}Hf values. This underscores the neutron-energy-dependence of n-capture by Hf nuclides.

Sample	Type/host	Group	μ^{178}Hf	$2\sigma_\mu$	μ^{180}Hf	$2\sigma_\mu$	*n*	CRE in Myr
AMS 004		A	8	9	−34	25	4	
AMS 001		A	8	8	26	21	3	
AMS 009		A	−1	17	−29	20	1	
AMS 027		A	14	17	−7	26	1	
AMS 041		A	2	5	−46	12	2	
AMS 003		A	7	7	−22	15	5	
AMS 032		A	15	17	−6	19	1	
AMS 053		A	14	17	−3	23	1	
AMS 008		A	9	17	−29	28	1	
AMS 040		A	16	4	16	30	3	
AMS 039		A	13	13	11	22	5	
AMS 013		A	17	10	4	14	3	
AMS 048 B		A	13	10	9	21	4	
AMS 007B		A	9	10	−13	35	2	
AMS 049		A	12	22	10	34	1	
AMS 054A		A	7	10	−8	41	2	
BCR-2		I	10	7	1	8	12	
BHVO-2		I	5	13	3	9	3	
AGV-2		I	3	7	6	8	11	
JG-2		I	4	9	3	17	4	
SE-3		I	20	58	5	93	1	
NZ 557		I	2	3	−2	6	35	
Allende	CV 3	C	−7	4	5	30	2	~5.4[1; 2]
El Hammami	H 5	C	9	10	−28	42	2	
Acfer 105	H 6	C	6	3	2	6	2	
Acfer 029	L 6	C	6	9	10	23	3	
DAG 275	CK 4/5	C	6	18	21	37	1	35.2[2]
DAG 137	CO 3	C	6	18	1	40	1	5.2–7.8[2, 3]
Acfer 301	H 4	C	2	14	19	38	1	
DAG 216	L 3	C	−5	20	−6	42	1	
DAG 318	H 3	C	−10	18	−6	43	1	
Acfer 066	LL 3–6	C	12	13	−10	27	2	25.1[4]
NWA 753	R 3.9	C	−2	21	−35	50	1	11[5]–25[6]
Murchison	CM 2	C	−6	7	−11	46	2	0.9–24[7]
Acfer 111	H 3–6	C	8	3	67	79	2	37.6–50.5[8]
DI 1	NWA 753	DI	6	12	−25	29	1	11[5]–25[6] (host)
DI 2	NWA 753	DI	−4	13	−5	29	1	11[5]–25[6] (host)
DI	Allende	DI	−22	23	−85	120	1	~5.4[1; 2] (host)
Peña Blanca Springs	Aubrite	Aubrite	−6	40	−14	88	1	72.1[9]–77[10]
VM B 1	Basaltic	MS	86	5	−178	3	4	133[11]–180[12]
VM B 2	Basaltic	MS	50	7	−120	15	1	133[11]–180[12]
VM B 3	Basaltic	MS	52	7	−123	14	1	133[11]–180[12]
VM B 4	Basaltic	MS	68	13	−143	25	1	133[11]–180[12]
VM B 5	Basaltic	MS	52	13	−105	14	1	133[11]–180[12]
VM G 1	Gabbroic	MS	73	19	−189	29	1	133[11]–180[12]
Estherville		MS	24	7	−84	27	2	63[13]–77[14]
Mincy		MS	−2	5	−26	50	2	44[14]
VM PX 1		MS	67	7	−157	32	2	133[11]–180[12]
VM PX 2		MS	55	11	−72	73	2	133[11]–180[12]
DAG 262.b.1	Lunar	Moon	153	14	−191	41	1	106[15]–1000[16]
CAI 4	Allende	CAI	−26	50	−78	151	1	~5.4[1; 2] (host)
CAI 2	Allende	CAI	26	7 (16)	35	21 (46)	3	~5.4[1; 2] (host)

that the Hf in these sample populations is indistinguishable with respect to r- and s-process contributions and shows no resolvable n-capture effects.

Surprisingly, the mean μ^{178}Hf values of the Archean gneisses ($+10\pm3$ ppm) and of all terrestrial rocks combined ($+7\pm3$ ppm) are positive and resolved from the standard solution (Fig. 1). This cannot be due to nucleosynthetic heterogeneity in r- or s-process because there is no associated positive deviation in μ^{180}Hf (-12 ± 12 ppm and -3 ± 7 ppm, respectively). Moreover, one post-Archean international rock standard (BCR-2; $+10\pm7$ ppm) also yields a positive mean μ^{178}Hf value precluding an explanation by heterogeneities in the early Earth.

Mass independent isotope fractionation effects related to differences in nuclear spin such as those reported for ^{177}Hf and ^{179}Hf (up to 129 ε-units using crown ethers; Fujii et al., 2001) can be ruled out because ^{178}Hf and ^{180}Hf have an identical nuclear spin of zero. Such effects would thus cause a positive correlation of μ^{178}Hf and μ^{180}Hf, which is not observed. No nuclear field shift effects resulting from nuclear volume differences have been found for Hf (Fujii et al., 2001).

From analytical tests (see Supplementary data), any bias resulting from the chemical separation of Hf can be excluded as the explanation for the positive μ^{178}Hf values. The non-mass-bias-corrected ^{179}Hf/^{177}Hf of sample and standard analyses at similar signal intensities can barely be resolved (Table S6). Thus, any effects of a

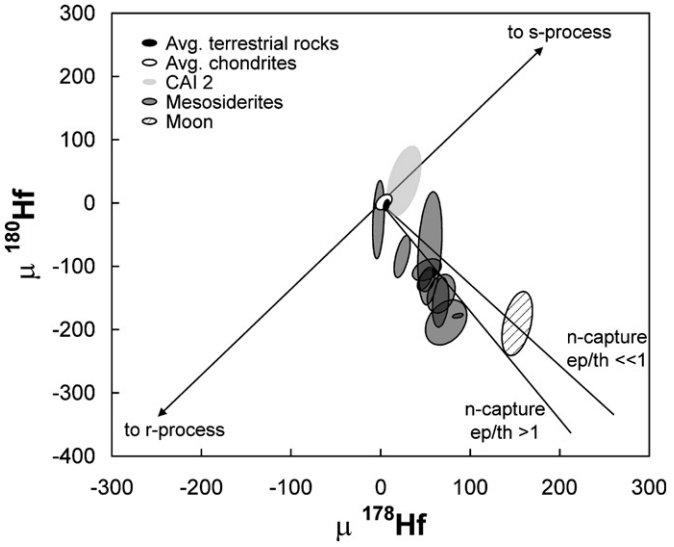

Fig. 3. Measured μ^{178}Hf vs. μ^{180}Hf of mesosiderites and the lunar meteorite DAG 262. Uncertainties for both are $2\sigma_\mu$ (see Section 2). Also shown are the average of chondrites, the average of terrestrial rocks, and CAI 2, shown at 95% confidence level. Trajectories illustrate the effects of n-capture at high ep/th >1 and ep/th ≪1 on 'normal' Hf and the results of mixing pure s- or r-process Hf with 'normal' Hf. Modelled trajectories are predicted 'measured' values that also incorporate the effects of a flawed mass-bias correction. All μ-values are calculated from mass-bias-corrected isotope compositions that were normalized to ^{179}Hf/^{177}Hf. On this scale, using the average Hf-isotope composition of acid-resistant phases from Murchison Yin et al. (2006) as a proxy for s-process Hf produces an identical trajectory. See the Supplementary data for further details concerning mixing and n-capture modelling.

mass-dependent fractionation that deviates from the exponential law (Russel et al., 1978; e.g., equilibrium fractionation) would be too small to create a bias between rock samples and solution standards.

Even after eliminating several potential sources of the positive μ^{178}Hf bias observed in some of the terrestrial rock samples, its origin remains unclear. We therefore placed more conservative limits on the analytical resolution for ^{178}Hf: A resolved positive μ^{178}Hf anomaly has to be higher than 13 (weighted mean of Archean gneisses plus the 95% confidence interval). The maximum degree of nucleosynthetic heterogeneity in the terrestrial and the chondrite data set is constrained from the observed range in μ^{180}Hf because the mean μ^{180}Hf of terrestrial samples seems to be free of bias. The population means of international rock standards, chondrites, and Archean gneisses and their 95% confidence limits span a range from −24 to +12 for μ^{180}Hf. To produce compositions outside this range (i.e., to produce resolvable anomalies), a ~19 ppm excess of pure s-process Hf or a ~26 ppm excess of pure r-process Hf is required. This would result in measured ^{176}Hf/^{177}Hf deviations between −0.6 and +0.3 ε-units including effects from the spurious mass-bias correction Given a typical external reproducibility for ^{176}Hf/^{177}Hf of 0.3 to 0.5 ε-units (for ~60 ng Hf per analysis) and uncertainties introduced by corrections for radiogenic ingrowth, such deviations would barely be resolvable.

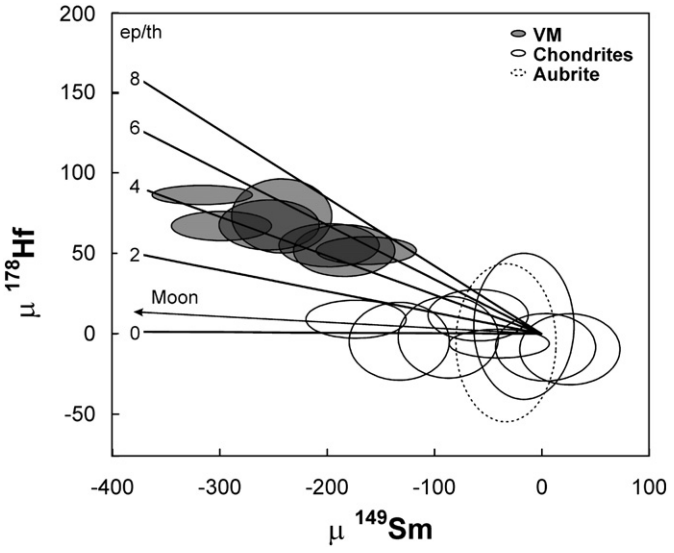

Fig. 4. Illustration of the coupled variations in measured μ^{178}Hf and μ^{149}Sm (i.e., comprising the effects of flawed mass-bias corrections using ^{179}Hf/^{177}Hf and ^{147}Sm/^{154}Sm) that result from n-capture at different ep/th (bold lines). Error ellipses are $2\sigma_\mu$. Assumed 'normal' Sm and Hf are used as a common starting point for the n-capture trajectories.

4.2. Potential nucleosynthetic heterogeneity in CAIs

The non-radiogenic stable Hf-isotope compositions of both CAIs measured in this study overlap with all data that are free of n-capture effects. Within significant uncertainties due to low Hf contents (total Hf: ~8 ng) an r-process excess cannot be excluded for CAI 4. However, at the 95% confidence limit, our data for CAI 2 ($n=3$) preclude any r-process excess and would even be consistent with an excess of as much as ~100 ppm pure s-process Hf (Fig. 3). Nucleosynthetic heterogeneity of this magnitude would produce a resolvable +1.5 ε-unit shift in the measured ^{176}Hf/^{177}Hf. In contrast, the initial ^{182}Hf/^{180}Hf of the solar system of $(9.72\pm0.44)\times10^{-5}$ (Burkhardt et al., 2008) would still remain a robust estimate within uncertainties.

4.3. Separate synthesis of heavy and light r-process nuclei

The lack of resolved nucleosynthetic r- and s-process anomalies in Hf reported here agrees with results for Sm and Nd (e.g., Andreasen and Sharma, 2006, 2007; Upadhyay and Mezger, 2008). However, it conflicts with findings of non-p-process nucleosynthetic heterogeneities in lighter elements such as Ba in carbonaceous chondrites (Andreasen and Sharma, 2007), Ni in CAIs, chondrites, and iron meteorites (Quitté et al. 2007; Regelous et al., 2008), Cr and Ti in CAIs, chondrites, and differentiated meteorites (Rotaru et al., 1992; Bogdanovski et al., 2002; Trinquier et al., 2007, 2009, Leya et al., 2008a, 2009), and Zr in CAIs (Schönbächler et al., 2003).

Trinquier et al. (2009) explained the solar system heterogeneity in Ti- and Cr-isotope compositions by thermal event(s) acting on a homogeneous proto-solar molecular cloud: In this model, preferential vaporization of thermally unstable carrier phases having s-process deficient (i.e., r-process enriched) isotope signatures produced vapor from which eventually CAIs formed. Consequently, the residual material would then have a variable s-process enrichment. Leya et al. (2009) have proposed trends among Zr-, Ni- and Ti-isotope anomalies in CAIs. Adopting the model of Trinquier et al. (2009) leaves two alternative explanations for our data: 1) The proposed thermal event(s) only vaporized 'normal' Hf, or 2) 'normal' Hf-isotope compositions were established during or after the thermal event(s). We expect no bias between our study and the Ti, Ni, and Zr studies from varying degrees of incomplete sample digestion because similar HF-HNO_3-based digestion techniques were applied in all studies. Case 1 appears unlikely because at least Hf and Zr but probably also Ti should reside in the same presolar carrier phases if they were synthesized together given that: a) the condensation temperatures of Ti and Zr bracket that of Hf and b) the most likely carrier phases of Zr and Hf are ZrO_2–HfO_2 solid solutions or various titanates (Lodders, 2003). Case 2 requires a fairly homogeneous addition of material containing r-excess Hf but no anomalous lighter nuclei ($\sim Z \leq 56$) and a mixing scenario in which the heterogeneity in the light nuclei remains preserved.

The combined Hf, Sm, Nd, Ba, Ni, Cr, Ti, and Zr data and the above considerations are consistent with an r-process synthesis of heavier nuclei that is separate from the synthesis of lighter nuclei ($Z \leq 56$; Andreasen and Sharma 2007; Qian and Wasserburg, 2007; Ott and Kratz, 2008). The data support models that explain the apparent deficit in the initial solar system abundance of ^{129}I relative to ^{182}Hf by separate additions of 'light' and 'heavy' r-process nuclides to the (proto) solar nebula (e.g., Qian and Wasserburg, 2007; Ott and Kratz, 2008). Observed 'heavy' r-process enriched element abundance patterns of extremely metal-poor stars (see e.g., Sneden et al., 2008) further substantiate these models. Thus, the presented data in conjunction with previously published data provide the first direct evidence for a separate addition of 'heavy' r-process Hf (*including* ^{182}Hf) and of lighter non-s-process nuclei (*including* ^{129}I) to the (proto) solar nebula. Possibly, nucleosynthetic anomalies found in W (one CAI, Burkhardt et al., 2008; iron meteorites, Qin et al., 2008) relate to the incorporation of W and Hf into different primary carrier phases. The stability of metal alloys (W carriers; Lodders, 2003) is sensitive to O_2-fugacities, which may have separated anomalous W from Hf during the distribution of carrier phases in the solar nebula. Identifying specific carrier phases of presolar components (e.g., Schönbächler et al., 2003, Reisberg et al. 2008; Trinquier et al. 2009) thus deserves continued attention.

4.4. Secondary neutron capture effects in mesosiderites, chondrites, an aubrite, and a lunar meteorite

The correlated deviation of ^{149}Sm/^{154}Sm and ^{150}Sm/^{154}Sm in mesosiderites, five chondrites, and Peña Blanca Springs clearly indicates that the Sm-isotope compositions have been modified by secondary n-capture (Fig. 2; e.g., Lingenfelter et al., 1972). This was expected for VM on the basis of cosmic-ray exposure ages of up to 180 Ma (Nagao and Bajo, 2006; Table 2), an estimated pre-atmospheric diameter of > 110 cm (Pedersen et al., 1992), and reported strong cosmic-ray exposure effects in Cl and noble gases (He, Ne, Ar, Begemann et al., 1976; Kr, Lavielle et al., 1998; Ar, Kr, Nagao and Bajo, 2006). The highly positive μ^{152}Sm of the gabbroic VM pebble resulting from n-capture on ^{151}Eu (σ_{th300K} of ~8120 barn; RI of ~3360 barn; see Nyquist et al., 1995; Rankenburg et al., 2006) reflects the extremely high Eu/Sm of gabbroic VM pebbles (Rubin and Mittlefehldt, 1992). The observed μ^{152}Sm of DAG 262 in conjunction with reported Eu/Sm values for lunar samples (e.g., Bischoff et al. 1998) enables us to model the maximum of the thermal neutron energy spectrum for the lunar meteorite DAG 262 (between 300 and 400 K, not shown). This is well within the range reported for other lunar samples (e.g., 200–400 K; Hidaka and Yoneda, 2007). The fact that μ^{178}Hf (Fig. 4) and μ^{180}Hf correlate with n-capture-induced Sm-isotope anomalies implies that the Hf isotope compositions were also affected by n-capture.

The correlated Hf and Sm-isotope signatures of the VM samples are closely matched by predictions for secondary n-capture effects. Modelling shows that the neutron energy spectra in the VM pebbles had higher epithermal-to-thermal ratios (ep/th ~3–8 at 300 K) than those in the chondrites, Peña Blanca Springs, and DAG 262, which all require ep/th <1. For spectra in which thermal neutrons dominate (i.e., ep/th <1) the production of resolvable non-radiogenic stable Hf anomalies (i.e., μ^{178}Hf >13 and μ^{180}Hf <−24) requires ~2.8×10^{15} thermal neutrons/cm^2 at 300 K. Such thermal fluences would produce a μ^{149}Sm value of ~−200. This explains the absence of resolved Hf-isotope anomalies even in those chondrites that show pronounced n-capture effects in ^{149}Sm/^{154}Sm and ^{150}Sm/^{154}Sm. Because Fe is a relatively inefficient neutron moderator and absorbs neutrons in the epithermal energy range (i.e., before they become thermal), higher epithermal neutron fluences above 1 eV and lower thermal neutron fluences are typical for Fe-rich target materials (Kollár et al., 2006). Thus, the deduced neutron energy spectra for VM reflect the Fe-dominated (~53 wt.%; at ~25 wt.% SiO_2) composition of mesosiderites. The variable Hf- and Sm-isotope anomalies in different VM samples indicate various ep/th. This could reflect a complex irradiation history, possibly including pre-irradiation in the VM parent body's regolith (see Hidaka et al., 2006) as has been proposed in a previous study (Nagao and Bajo, 2006). Alternatively, the variable ep/th for various pebbles may have resulted from various shielding depths and iron contents. This issue cannot be resolved because the spatial context of the individual samples cannot be reconstructed.

In addition to revealing n-capture effects, the combined μ^{178}Hf and μ^{180}Hf pattern of the mesosiderite samples may also indicate variable degrees of mixing between 'normal' Hf with an end-member Hf composition predicted by some neutron-burst models (e.g., $T_9 = 0.98$; Meyer and Adams, 2006; T_9 = temperature in 10^9K; not shown). Even the correlation between μ^{178}Hf and μ^{149}Sm would be consistent with variable contributions of n-burst material to VM (not shown). However, an analogous mixing model for Sm produces a trend that is almost perpendicular to the observed n-capture-induced correlation between ^{149}Sm/^{154}Sm and ^{150}Sm/^{154}Sm (Fig. 2). Therefore, n-capture reactions rather than contributions from an n-burst component are a plausible explanation for the combined Hf and Sm-isotope anomalies.

4.5. Hafnium isotopes as a possible monitor for epithermal neutron capture

Given the importance of n-capture reactions for interpreting e.g., W-isotope data, good proxies for the thermal and epithermal neutron fluences are needed. The sensitivity of the Hf-isotope composition to epithermal n-capture makes Hf a suitable monitor for such reactions. When correcting for n-capture effects, the spectra and the fluence of the neutrons (thermal and epithermal) should be known for the entire exposure history. However, the exposure history might have been complex and may include neutron irradiation on the surface of the parent body. Being *refractory* elements, Hf, Gd, Sm, and Eu are ideally suited for such applications. In contrast, given their volatility, noble gases (Rowe et al., 1965, Albee et al., 1970) or Cd (Wombacher et al. 2008) may only provide a fragmentary n-capture history. This is supported by reported inconsistencies between the cosmic-ray exposure histories concluded from noble gas data and determinations of neutron fluences based on Sm-isotope analyses (e.g., Hidaka et al., 1999). Moreover, cosmogenic noble gases are also produced by reactions other than neutron capture (e.g., Leya et al., 2008b) and may record irradiation at different energies (e.g., Eugster et al., 1993). Leya et al. (2003) have shown the great potential of combined Sm-, Gd-, and W-isotope studies for the correction of cosmic-ray-induced shifts in W-isotope compositions. It is proposed here that integrating the analysis of the non-radiogenic stable Hf-isotope composition will further refine this approach by providing additional information on neutron energy spectra. Improved predictions are expected for cosmogenic nuclide production and burnout especially for high-Fe samples such as H-chondrites, stony iron meteorites, and iron meteorites. Further constraints on neutron energy spectra may be provided by isotope compositions of other elements having nuclides that possess significant but highly unequal epithermal and thermal neutron capture probabilities (e.g., RI $\gg \sigma_{th}$: ^{109}Ag, ^{115}In, ^{123}Te, ^{162}Dy, ^{163}Dy, ^{167}Er, ^{168}Yb, ^{185}Re; RI $\ll \sigma_{th}$: ^{113}Cd, ^{151}Eu, ^{164}Dy).

Recently, σ_{th} and RI for ^{182}Hf have been determined (133 ± 10 and 5850 ± 660 barn, respectively, Vockenhuber et al., 2008). Using these values, we can estimate the influence of the burnout of ^{182}Hf on the Hf–W chronometer. For an irradiation similar to that inferred for VM B 1 during the lifetime of ^{182}Hf, a maximum of 0.01% of the total ^{182}Hf would have undergone n-capture to ^{183}Hf with subsequent β-decay to ^{183}W instead of decay to ^{182}W. Even for samples having extremely high Hf/W (e.g., zircon with Hf/W up to ~195,000, Srinivasan et al.,

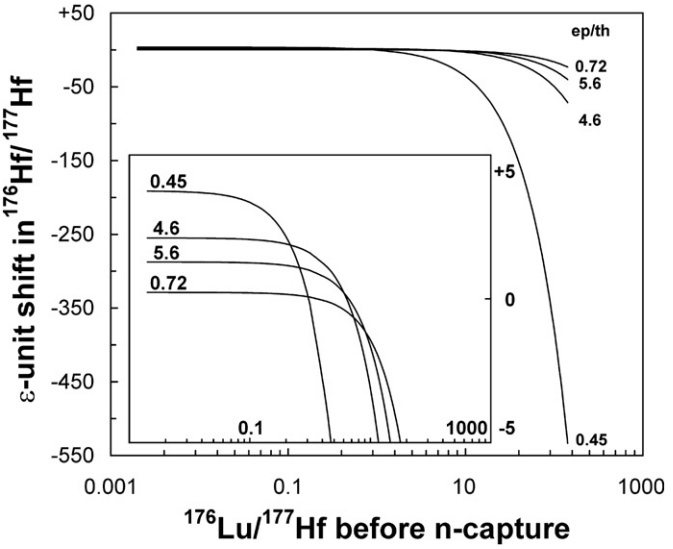

Fig. 5. Schematic illustration of the shift in measured, $^{179}Hf/^{177}Hf$-normalized $^{176}Hf/^{177}Hf$ resulting from n-capture for different $^{176}Lu/^{177}Hf$, as well as thermal fluences (Ψ_{th}) and ep/th as deduced for four samples. The shift is given in ε-units relative to the 'non-irradiated' composition. Equivalent samples from top to bottom (outer diagram) and respective Ψ_{th} in n/cm²: El Hammami: 2.4×10^{15} (i.e., a sample that has no resolved non-radiogenic stable Hf-isotope anomalies); VM B 4: 1.9×10^{15}; VM B 1–3.8×10^{15}; DAG 262: 6.2×10^{16}; numbers at ends of curves: ep/th. Inset: Close-up of outer diagram for ε-unit shift in $^{176}Hf/^{177}Hf$ from −5 to +5, illustrating the effects at typical whole-rock Lu/Hf (≪0.1); numbers above the curves: ep/th.

2007), this would result in a maximum shift in $^{182}W/^{184}W$ of about one ε-unit if the zircon formed at the beginning of the solar system and all n-capture occurred immediately. Hence, at these neutron fluences, the n-capture-induced burnout of ^{182}Hf cannot introduce a significant bias into Hf–W chronometry. Note that we do not expect any substantial thermal and epithermal neutron fluences in the early solar system because of the presumably low density of the solar nebula, which would have resulted in relatively long timescales between production, scattering, and capture of neutrons. Consequently, neutrons would be expected to decay ($T_{1/2}=10.23$ min; Amsler et al., 2008) before being thermalized and captured.

4.6. Implications of neutron capture reactions for ^{176}Lu–^{176}Hf chronology and geochemistry

N-capture reactions can modify Hf-isotope abundances. Assuming the same for the Lu isotopes, it is important to evaluate the expected effects on $^{176}Hf/^{177}Hf$ and $^{176}Lu/^{177}Hf$, which are critical for chronology. The effects of n-capture on hypothetical 'samples' that lie on a 4.567 Ga isochron, have a chondritic initial $^{176}Hf/^{177}Hf$ value, and whose $^{176}Lu/^{177}Hf$ values range from 0.002 to 142 have been modelled. This range in $^{176}Lu/^{177}Hf$ is reasonable for meteoritic material. For example, the maximum value of 142 matches the highest $^{176}Lu/^{177}Hf$ ratio yet reported for meteoritic mineral phases (i.e., phosphates; Amelin, 2005). A schematic illustration of the shift in measured $^{176}Hf/^{177}Hf$ resulting from n-capture for various Lu/Hf, ep/th, and thermal neutron doses is given in Fig. 5. In the model, we used irradiation scenarios with a neutron temperature of 300 K, which are similar to that deduced for our samples (see Table 3 and Supplementary data).

The results are summarized as follows: For *Lu/Hf typical of bulk meteorites*, significant neutron capture will result in an overestimation of $^{176}Hf/^{177}Hf$ (i.e., measured $^{176}Hf/^{177}Hf$>true $^{176}Hf/^{177}Hf$>non-irradiated $^{176}Hf/^{177}Hf$) without producing resolvable shifts in $^{176}Lu/^{177}Hf$. The overestimation of $^{176}Hf/^{178}Hf$ comes primarily from *epithermal* n-capture by ^{177}Hf and ^{178}Hf and increases with increasing *epithermal* neutron fluences. *At very high-Lu/Hf* (e.g., in phosphates), the *thermal* n-capture-induced burnout of ^{176}Lu (eventual feeding of ^{177}Hf) dominates. This results in an underestimation of $^{176}Hf/^{177}Hf$ (i.e., measured $^{176}Hf/^{177}Hf$<true $^{176}Hf/^{177}Hf$<non-irradiated $^{176}Hf/^{177}Hf$) and a resolvable increase in the obtained $^{176}Lu/^{177}Hf$. Both effects increase with increasing *thermal* neutron fluences and increasing Lu/Hf. Spike stripping only introduces a significant error into $^{176}Hf/^{177}Hf$ determinations (>+0.3 ε-unit shift) at $^{176}Lu/^{177}Hf$>50 and neutron fluences at least as high as deduced for the lunar meteorite DAG 262. Using a factor of 2 higher Yb cross sections and RIs would not significantly

Table 3
Results of n-capture modelling. Ψ_{th}: integrated thermal neutron flux in n/cm²; non-irradiated: hypothetical composition before n-capture; 'unspiked' MB corrected: corrected for mass bias, i.e., modelled measured ratio incorporating the effects of shifted normalizing ratios on a spike-free analysis; 'spike stripped': modelled measured ratio incorporating the effects of shifted normalizing ratios on a spiked analysis. All models were calculated for 300 K.

Fluence is equal to that of this sample:	Ψ_{th}	ep/th	Non-irradiated $^{176}Lu/^{177}Hf$	Non-irradiated $^{176}Hf/^{177}Hf$	After n-capture 'unspiked' MB corrected $^{176}Hf/^{177}Hf$	ε-unit error in $^{176}Hf/^{177}Hf$	After n-capture 'spike stripped' $^{176}Lu/^{177}Hf$	ε-unit error in $^{176}Lu/^{177}Hf$	After n-capture 'spike stripped' $^{176}Hf/^{177}Hf$	ε-unit error in $^{176}Hf/^{177}Hf$	ε-unit error in $^{176}Hf/^{177}Hf$ vs. unspiked
VM B 1	3.8×10^{15}	4.6	0.002000	0.279995	0.280054	+2.1	0.002000	−0.3	0.280054	+2.1	+0.01
VM B 1	3.8×10^{15}	4.6	0.03000	0.282487	0.282546	+2.1	0.03000	−0.2	0.282547	+2.1	+0.01
VM B 1	3.8×10^{15}	4.6	0.1500	0.293168	0.293227	+2.0	0.1500	−0.2	0.293228	+2.0	+0.01
VM B 1	3.8×10^{15}	4.6	10.00	1.16988	1.16951	−3.1	10.00	+5	1.16952	−3.1	0.00
VM B 1	3.8×10^{15}	4.6	100.0	9.18047	9.13474	−50	100.5	+47	9.13481	−50	+0.08
VM B 1	3.8×10^{15}	4.6	142.0	12.9187	12.8263	−71	143.0	+67	12.8265	−71	+0.12
DAG 262	6.2×10^{16}	0.45	0.002000	0.279995	0.280099	+3.7	0.001999	−3	0.280100	+3.7	+0.02
DAG 262	6.2×10^{16}	0.45	0.03000	0.282487	0.282589	+3.6	0.02999	−2	0.282590	+3.6	+0.02
DAG 262	6.2×10^{16}	0.45	0.1500	0.293168	0.29326	+3.1	0.1500	−2	0.293260	+3.2	+0.02
DAG 262	6.2×10^{16}	0.45	10.00	1.16988	1.16569	−36	10.03	+34	1.16569	−36	+0.02
DAG 262	6.2×10^{16}	0.45	100.0	9.18047	8.83139	−380	103.5	+345	8.83198	−380	+0.67
DAG 262	6.2×10^{16}	0.45	142.0	12.9187	12.2285	−534	148.8	+482	12.2297	−533	+1.00
VM B 4	1.9×10^{15}	5.6	0.002000	0.279995	0.280031	+1.3	0.002000	−0.1	0.280031	+1.3	+0.01
VM B 4	1.9×10^{15}	5.6	0.03000	0.282487	0.282523	+1.3	0.0300	−0.1	0.282523	+1.3	+0.01
VM B 4	1.9×10^{15}	5.6	0.1500	0.293168	0.293204	+1.2	0.1500	−0.1	0.293204	+1.2	+0.01
VM B 4	1.9×10^{15}	5.6	10.00	1.16988	1.16968	−1.7	10.00	+3	1.16968	−1.7	0.00
VM B 4	1.9×10^{15}	5.6	100.0	9.18047	9.15481	−28	100.3	+27	9.15485	−28	+0.05
VM B 4	1.9×10^{15}	5.6	142.0	12.9187	12.8668	−40	142.5	+38	12.8669	−40	+0.07
El Hammami	2.4×10^{15}	0.72	0.002000	0.279995	0.280001	+0.22	0.002000	−0.1	0.280001	+0.22	0.00
El Hammami	2.4×10^{15}	0.72	0.03000	0.282487	0.282493	+0.22	0.0300	−0.1	0.282493	+0.22	0.00
El Hammami	2.4×10^{15}	0.72	0.1500	0.293168	0.293174	+0.20	0.1500	−0.1	0.293174	+0.2	0.00
El Hammami	2.4×10^{15}	0.72	10.00	1.16988	1.16971	−1.4	10.00	+1	1.16971	−1.4	0.00
El Hammami	2.4×10^{15}	0.72	100.0	9.18047	9.16551	−16	100.2	+15	9.16553	−16	+0.03
El Hammami	2.4×10^{15}	0.72	142.0	12.9187	12.8887	−23	142.3	+21	12.8887	−23	+0.04

change the model results for typical whole-rock Lu/Hf. However, at highly elevated Lu/Hf, the modelled effects will be magnified. In a worst case scenario, i.e., a $^{176}Lu/^{177}Hf$ of 142 and a neutron exposure similar to DAG 262, the shifts in measured $^{176}Hf/^{177}Hf$ and $^{176}Lu/^{177}Hf$ would be magnified by ~4.2% and ~4.3%. Thus, secondary n-capture can decrease the slopes of Lu–Hf meteorite isochrons if high-Lu/Hf phases are included. However, these are Hf-poor accessory phases which limits the possible precision of $^{177}Hf/^{177}Hf$ analyses (2σ of 0.50 to 7.53%; Amelin, 2005; as opposed to 0.3 to 0.5 ε-units for whole meteorite samples). Therefore, if a single fraction of a high-Lu/Hf phase is included in an isochron, n-capture effects will mainly be masked by analytical uncertainties. Isochrons comprising multiple high-Lu/Hf fractions have to be evaluated individually. For example, multiple phosphate fractions of the Richardton chondrite (H5; ^{207}Pb–^{206}Pb age: 4.5507 Ga; Amelin et al., 2005) yield a Lu–Hf isochron with an age of 4545 ± 36 Ma and an initial $^{176}Hf/^{177}Hf$ of 0.2792 ± 0.0019 (MSWD = 0.55; Amelin, 2005). Had Richardton had the same irradiation history as VM B 1, a respective 'non-irradiated' isochron would give an age of 4560 ± 37 Ma at an initial $^{176}Hf/^{177}Hf$ of 0.2789 ± 0.0019 (MSWD = 0.67) using analytical uncertainties from Amelin (2005) and assuming no error correlation between $^{176}Hf/^{177}Hf$ and $^{176}Lu/^{177}Hf$. Hence, for this scenario, neither age nor the initial $^{176}Hf/^{177}Hf$ value would be affected significantly. This changes when including 'bulk' meteorite data for Richardton (Patchett et al., 2004). In this case, the Lu–Hf age is 4540 ± 34 Ma and the initial $^{176}Hf/^{177}Hf$ is 0.279849 ± 0.000032 (MSWD = 0.53). Assuming the same neutron irradiation history as above, the 'non-irradiated' isochron would yield a Lu–Hf age of 4553 ± 34 Ma and an initial $^{176}Hf/^{177}Hf$ of 0.279781 ± 0.000032. Unrecognized n-capture could thus cause an overestimation of the initial $^{176}Hf/^{177}Hf$ value of a meteorite. Note that these are hypothetical examples: There neither is any evidence for such neutron irradiation in Richardton, nor would neutron irradiation at ep/th <1 that is not resolvable by Hf-isotope analyses (Section 4.4) affect age or initial $^{176}Hf/^{177}Hf$ of the Richardton isochron significantly.

Variable n-capture effects in different meteorites can induce scatter and alter the slopes of whole-rock meteorite isochrons. However, to increase the slope of such an isochron significantly, the n-capture effect in each sample fortuitously would have to be proportional to its Lu/Hf, an extremely unlikely condition. So far, no n-capture effects in Hf have been observed in chondrites. The maximum error in $^{176}Hf/^{177}Hf$ for unresolved neutron irradiation (with respect to Hf-isotope analyses) at ep/th < 1 and $^{176}Lu/^{177}Hf$ typical for whole meteorites would be +0.35 ε-units. N-capture therefore cannot explain the discrepancy between ^{176}Lu decay constant determinations using terrestrial (e.g., Scherer et al., 2001) and meteoritic materials (e.g., Bizzarro et al., 2003). It can, however, affect the initial $^{176}Hf/^{177}Hf$ values of meteorite whole-rock and internal mineral isochrons. If not recognized, this may produce incorrect estimates of initial $^{176}Hf/^{177}Hf$ values of meteorites, planetary bodies, and the solar system. Hence, spurious, low and high chondritic model ages may result from neutron irradiation of samples from 'enriched' and 'depleted' sources, respectively. A better knowledge of the depth- and composition-dependence of secondary neutron energy spectra would greatly contribute to a better quantification of such effects.

5. Conclusions

Based on our data, the non-radiogenic stable Hf-isotope compositions of chondrites and terrestrial rocks are indistinguishable. Hence, for Hf there is no evidence for nucleosynthetic heterogeneity in Earth and chondrites and r- or s-process excesses are limited to ~26 ppm and ~19 ppm, respectively. These translate into possible associated shifts in measured $^{176}Hf/^{177}Hf$ between −0.6 and +0.3 ε-units. The lack of resolvable nucleosynthetic anomalies in Hf-isotope compositions supports an r-process synthesis of Hf that was separate from that of lighter elements such as Zr, Ti, Cr, or Ni, for which such anomalies have been reported.

Secondary neutron-capture, especially in the epithermal energy range, can significantly modify the Hf-isotope composition of meteorites as demonstrated for mesosiderites and one lunar meteorite. Neutron-capture reactions can also affect Lu–Hf chronology. At Lu/Hf typical for whole rocks, epithermal n-capture may significantly increase the measured $^{176}Hf/^{177}Hf$. These apparent $^{176}Hf/^{177}Hf$ excesses are not supported by the decay of ^{176}Lu and would thus produce spuriously high initial $^{176}Hf/^{177}Hf$ values. However, neutron-capture-induced deviations in the Hf-isotope composition have not been identified in chondrites yet. Thus, neutron-capture effects cannot account for the observed ^{176}Lu decay constant discrepancy between terrestrial and extra-terrestrial materials.

For reliable interpretations of $^{176}Hf/^{177}Hf$ and ^{176}Lu–^{176}Hf data of extra-terrestrial samples, assessing their stable non-radiogenic Hf-isotope composition is important. The limited data set presented here does not preclude the use of a chondritic ^{176}Lu–^{176}Hf reference scheme for the Bulk Silicate Earth and the bulk silicate portions of other planetary bodies. However, effects on the ^{176}Lu–^{176}Hf system due to variation in the p-process contribution to different solar system objects are unknown and deserve future attention.

Acknowledgments

We are grateful to the following people who helped make this study possible: Addi Bischoff generously provided most of the meteorite samples as well as his expertise during their selection. Wouter Bleeker was our mentor when sampling the Archean Gneisses used in this project. Carolyn Relf, John Ketchum, and Tom Chacko provided the major infrastructure during field work. Oliver Plümper was instrumental in the preparation of the Archean gneiss samples. Toni Schulz has shared digestions of Mincy and Estherville. Special thanks are due to Heidi Baier, Michael Feldhaus, and Frank Deipenwisch for their ongoing efforts in maintaining and constantly improving the analytical infrastructure at Münster. PS thanks Andreas Stracke, Ben C. Reynolds, Christoph Burkhardt, Nadia Vogel, and Thorsten Kleine for discussions. Constructive and helpful comments by two anonymous reviewers, Hiroshi Hidaka and the editor Rick Carlson were appreciated and helped improve the manuscript. This work was funded by the German Research Foundation (DFG, ME 1717/18-1).

Appendix A. Supplementary data

Supplementary data associated with this article can be found, in the online version, at doi:10.1016/j.epsl.2010.02.050.

References

Albarède, F., Scherer, E.E., Blichert-Toft, J., Rising, M.T., Simionovici, A., Bizzarro, M., 2006. Gamma-ray irradiation in the early solar system and the conundrum of the ^{176}Lu decay constant. Geochim. et Cosmochim. Acta 70, 1261–1270.

Albee, A.L., Burnett, D.S., Chodos, A.A., Eugster, 0.J., Huneke, J.C., Papanastassiou, D.A., Podosek, F.A., Price Russ II, G., Sanz, H.G., Tera, F., Wasserburg, G.J., 1970. Ages, irradiation history, and chemical composition of lunar rocks from the sea of tranquility. Science 167, 463–466.

Albrecht, A., Schnabel, C., Vogt, S., Xue, S., Herzog, G.F., Begemann, F., Weber, H.W., Middleton, R., Fink, D., Klein, J., 2000. Light noble gases and cosmogenic radionuclides in Estherville, Budulan and other mesosiderites: implications for exposure histories and production rates. Meteor. Planet. Sci. 35, 975–986.

Amelin, Y., 2005. Meteorite phosphates show constant ^{176}Lu decay rate since 4557 million years ago. Science 310, 839–841.

Amelin, Y.V., Lee, D.C., Halliday, A.N., Pidgeon, R.T., 1999. Nature of the Earth's earliest crust from hafnium isotopes in single detrital zircons. Nature 399, 252–255.

Amelin, Y., Ghosh, A., Rotenberg, E., 2005. Unravelling the evolution of chondrite parent asteroids by precise U–Pb dating and thermal modelling. Geochim. et Cosmochim. Acta 69, 505–518.

Amsler, C., et al., 2008. Review of particle physics — summary tables of particle properties. Phys. Lett. B 667, 31–100.

Andreasen, R., Sharma, M., 2006. Solar nebula heterogeneity in p-process samarium and neodymium isotopes. Science 314, 806–809.

Andreasen, R., Sharma, M., 2007. Mixing and homogenization in the early solar system: clues from Sr, Ba, Nd, and Sm isotopes in meteorites. Astrophys. J. 665, 874–883.
Arnould, A., Goriely, S., 2003. The p-process of stellar nucleosynthesis: astrophysics and nuclear physics status. Phys. Rep. 384, 1–84.
Arnould, A., Goriely, S., Takahashi, K., 2007. The r-process of stellar nucleosynthesis: astrophysics and nuclear physics achievements and mysteries Phys. Rep. 450, 97–213.
Begemann, F., Weber, H.W., Vilcsek, E., Hintenberger, H., 1976. Rare gases and ^{36}Cl in stony-iron meteorites: cosmogenic elemental production rates, exposure ages, diffusion losses and thermal histories. Geochim. et Cosmochim. Acta 40, 353–368.
Bischoff, A., Weber, D., Clayton, R.N., Faestermann, T., Franchi, I.A., Herpers, U., Knie, K., Korschinek, G., Kubik, P.W., Mayeda, T.K., Merchel, S., Michel, R., Neumann, S., Palme, H., Pillinger, C.T., Schultz, L., Sexton, A.S., Spettel, B., Verchovsky, A.B., Weber, H.W., Weckwerth, G., Wolf, D., 1998. Petrology, chemistry, and isotopic compositions of the Lunar highland regolith breccia Dar al Gani 262. Meteor. Planet. Sci. 33, 1243–1257.
Bizzarro, M., Baker, J.A., Haack, H., Ulfbeck, D., Rising, M., 2003. Early history of the Earth's crust–mantle system inferred from hafnium isotopes in chondrites. Nature 421, 931–933.
Bizzarro, M., Ulfbeck, D., Trinquier, A., Thrane, K., Connelly, J.N., Meyer, B.S., 2007. Evidence for a late supernova injection of ^{60}Fe into the protoplanetary disk. Science 316, 1178–1181.
Blichert-Toft, J., Albarède, F., 1997. The Lu–Hf isotope geochemistry of chondrites and the evolution of the mantle–crust system. Earth Planet. Sci. Lett. 148, 243–258.
Bogdanovski, O., Papanastassiou, D.A., Wasserburg, G.J., 2002. Cr isotopes in Allende Ca–Al-rich inclusions. Lunar Planet. Sci. 33, 1802.
Bouvier, A., Vervoort, J.D., Patchett, P.J., 2008. The Lu–Hf and Sm–Nd isotopic composition of CHUR: constraints from unequilibrated chondrites and implications for the bulk composition of terrestrial planets. Earth Planet. Sci. Lett. 273, 48–57.
Burkhardt, C., Kleine, T., Bourdon, B., Palme, H., Zipfel, J., Friedrich, J.M., Ebel, D.S., 2008. Hf–W mineral isochron for Ca,Al-rich inclusions: age of the solar system and the timing of core formation in planetesimals. Geochim. et Cosmochim. Acta 72, 6177–6197.
Busso, M., Gallino, R., Wasserburg, G.J., 1999. Nucleosynthesis in asymptotic giant branch stars: relevance for galactic enrichment and solar system formation. Ann. Rev. Astron. Astrophys. 37, 239–309.
Carlson, R.W., Boyet, M., Horan, M., 2007. Chondrite barium, neodymium, and samarium isotopic heterogeneity and early Earth differentiation. Science 316, 1175–1178.
Ebisawa, N., Park, J., Nagao, K., 2003. Noble gases in Northwest Africa 753 (NWA 753), Rumuruti chondrites. Geochim. et Cosmochim. Acta 67, A84.
Eugster, O., Michel, T., Niedermann, S., Wang, D., Yi, W., 1993. The record of cosmogenic, radiogenic, fissiogenic, and trapped noble gases in recently recovered Chinese and other chondrites. Geochim. et Cosmochim. Acta 57, 1115–1142.
Eugster, O., Polnau, E., Salerno, E., Terribilini, D., 2000. Lunar surface exposure models for meteorites Elephant Moraine 96008 and Dar al Gani 262 from the Moon. Meteor. Planet. Sci. 35, 1177–1181.
Eugster, O., Lorenzetti, S., Krähenbühl, U., Marti, K., 2007. Comparison of cosmic-ray exposure ages and trapped noble gases in chondrule and matrix samples of ordinary, enstatite, and carbonaceous chondrites. Meteor. Planet. Sci. 42, 1351–1371.
Fernandes, V.A., Burgess, R., Turner, G., 2000. Laser argon-40–argon-39 age studies of Dar al Gani 262 lunar meteorite. Meteor. Planet. Sci. 35, 1355–1364.
Fujii, T., Moriyama, H., Hirata, T., Nishizawa, K., 2001. Isotope effects of hafnium in solvent extraction using crown ethers. Bull. Chem. Soc. Jpn. 74, 1031–1032.
Gosse, J.C., Phillips, F.M., 2001. Terrestrial in situ cosmogenic nuclides: theory and application. Quat. Sci. Rev. 1475–1560.
Hidaka, H., Yoneda, S., 2007. Sm and Gd isotopic shifts of Apollo 16 and 17 drill stem samples and their implications for regolith history. Geochim. et Cosmochim. Acta 71, 1074–1086.
Hidaka, H., Ebihara, M., Yoneda, S., 1999. High fluences of neutrons determined from Sm and Gd isotopic compositions in aubrites. Earth Planet. Sci. Lett. 173, 41–51.
Hidaka, H., Ebihara, M., Yoneda, S., 2000. Isotopic study of neutron capture effects on Sm and Gd in chondrites. Earth Planet. Sci. Lett. 180, 29–37.
Hidaka, H., Ohta, Y., Yoneda, S., 2003. Nucleosynthetic components of the early solar system inferred from Ba isotopic compositions in carbonaceous chondrites. Earth Planet. Sci. Lett. 214, 455–466.
Hidaka, H., Yoneda, S., Marti, K., 2006. Regolith history of the aubritic meteorite parent body revealed by neutron capture effects on Sm and Gd isotopes. Geochim. et Cosmochim. Acta 70, 3449–3456.
Jäckel, A., Romstedt, J., Bischoff, A., 1997. Acfer 066 (LL3-6) petrologic and track study of a spectacular regolith breccia. Lunar Planet. Sci. 28, 645.
Klay, N., Käppeler, F., Beer, H., Schatz, G., 1991. Nuclear structure of ^{176}Lu and its astrophysical consequences. II: ^{176}Lu, a thermometer for stellar helium burning. Phys. Rev C 44, 2839–2849.
Kollár, D., Michel, R., Masarik, J., 2006. Monte Carlo simulations of GCR neutron capture production of cosmogenic nuclides in stony meteorites and lunar surface. Meteor. Planet. Sci. 41, 375–389.
Lavielle, B., Gilabert, E., Soares, M.R., Vasconcellos, M.A.Z., Poupeau, G., Canut de Bon, C., Cisternas, M.E., Scorzelli, R.B., 1998. Noble gases and metal studies in the Vaca Muerta mesosiderite. Meteorit. Planet. Sci. 33 Abs. # 5122.
Leya, I., 1997. Modellrechnungen zur Beschreibung der Wechselwirkungen galaktischer kosmischer Teilchenstrahlung mit Stein- und Eisenmeteoroiden. Dissertation, Universität Hannover. 459 pp.
Leya, I., Wieler, R., Halliday, A.N., 2000. Cosmic-ray production of tungsten isotopes in lunar samples and meteorites and its implications for Hf–W cosmochemistry. Earth Planet. Sci. Lett. 175, 1–12.
Leya, I., Wieler, R., Halliday, A.N., 2003. The influence of cosmic-ray production on extinct nuclide systems. Geochim. et Cosmochim. Acta. 67, 529–541.
Leya, I., Schönbächler, M., Wiechert, U., Krähenbühl, U., Halliday, A.N., 2008a. Titanium isotopes and the radial heterogeneity of the solar system. Earth Planet. Sci. Lett. 266, 233–244.
Leya, I., David, J.-C., Leray, S., Wieler, R., Michel, R., 2008b. Production of noble gas isotopes by proton-induced reactions on bismuth. Nucl. Instr. and Meth. B 266, 1030–1042.
Leya, I., Schönbächler, M., Krähenbühl, U., Halliday, A.N., 2009. New titanium isotope data for Allende and Efremovka CAIs. Astrophys. J. 702, 1118–1126.
Lingenfelter, R.E., Canfield, E.H., Hampel, V.E., 1972. The lunar neutron flux revisited. Earth Planet. Sci. Lett. 16, 355–369.
Lodders, K., 2003. Solar system abundances and condensation temperatures of the elements. Astrophys. J. 591, 1220–1247.
Lorenzetti, L., Eugster, O., Busemann, H., Marti, K., Burbine, T.H., McCoy, T., 2003. History and origin of aubrites. Geochim. et Cosmochim. Acta 67, 557–571.
Maréchal, C.N., Télouk, P., Albarède, F., 1999. Precise analysis of copper and zinc isotopic compositions by plasma-source mass spectrometry. Chem. Geol. 156, 251–273.
Meyer, B.S., Adams, D.C., 2006. Neutron burst production of ^{60}Fe necessarily implies production of ^{182}Hf. Lunar Planet. Sci. 37, 1402.
Meyer, B.S., The, L.-S., Johnson, J., 2008. Nuclear effects of supernova-accelerated cosmic rays on early solar system planetary bodies. Lunar Planet. Sci. 39, 2194.
Miura, Y.N., Hidaka, H., Nishiizumi, K., Kusakabe, M., 2007. Noble gas and oxygen isotope studies of aubrites: a clue to origin and histories. Geochim. et Cosmochim. Acta 71, 251–270.
Münker, C., Weyer, S., Scherer, E.E., Mezger, K., 2001. Separation of high field strength elements (Nb, Ta, Zr, Hf) and Lu from rock samples for MC-ICPMS measurements. Geochem. Geophys. Geosyst. 2. doi:10.1029/2001GC000183.
Nagao, K., Bajo, K., 2006. Complex exposure history of Vaca Muerta mesosiderite inferred from noble gases. Meteorit. Planet. Sci. 41 Abs. # 5218.
Nyquist, L.E., Wiesman, H., Bansal, B., Shih, C.-Y., Keith, J.E., Harper, C.L., 1995. ^{146}Sm–^{142}Nd formation interval for the lunar mantle material. Geochim. et Cosmochim. Acta 59, 2817–2837.
Ott, U., Kratz, K.-L., 2008. Meteoritic evidence for two r-processes and the HEW scenario. New Astron. Rev. 52, 396–400.
Palme, H., Jones, A., 2007. Solar system abundances of the elements. In: Holland, H.D., Turekian, K.K. (Eds.), Treatise on Geochemistry. Elsevier Sci. Publ. Co, Amsterdam, pp. 41–61. Chapter 1.03.
Patchett, P.J., 1983. Importance of the Lu–Hf isotopic system in studies of planetary chronology and chemical evolution. Geochim. et Cosmochim. Acta 47, 81–91.
Patchett, P.J., Tatsumoto, M., 1980. Lu–Hf total-rock isochron for the eucrite meteorites. Nature 288, 571–574.
Patchett, P.J., Vervoort, J.D., Söderlund, U., Salters, V.J.M., 2004. Lu–Hf and Sm–Nd isotopic systematics in chondrites and their constraints on the Lu–Hf properties of the Earth. Earth Planet. Sci. Lett. 222, 29–41.
Pedersen, H., de Bon, C.C., Lindgren, H., 1992. Vaca Muerta mesosiderite strewnfield. Meteoritics 27, 126–135.
Pedroni, A., Begemann, F., 1994. On unfractionated solar noble gases in the H3-6 meteorite Acfer 111. Meteoritics 29, 632–642.
Qian, Y.-Z., Wasserburg, G.J., 2008. Where, oh where has the r-process gone? Phys. Rep. 442, 237–268.
Qin, L., Dauphas, N., Wadhwa, M., Markowski, A., Gallino, R., Janney, P.E., Bouman, C., 2008. Tungsten nuclear anomalies in planetesimal cores. Astrophys. J. 674, 1234–1241.
Quitté, G., Halliday, A.N., Meyer, B.S., Markowski, A., 2007. Correlated iron 60, nickel 62, and zirconium 96 in refractory inclusions and the origin of the solar system. Astrophys. J. 655, 678–684.
Rankenburg, K., Brandon, A.D., Neal, C.R., 2006. Neodymium isotope evidence for a chondritic composition of the moon. Science 312, 1369–1372.
Regelous, M., Elliott, T., Coath, C.D., 2008. Nickel isotope heterogeneity in the early solar system. Earth Planet. Sci. Lett. 272, 330–338.
Reisberg, L., Dauphas, N., Luguet, A., Pearson, D.G., Gallino, R., Zimmermann, C., 2008. Nucleosynthetic osmium isotope anomalies in acid leachates of the Murchison meteorite. Earth Planet. Sci. Lett. 277, 334–344.
Rotaru, M., Birck, J.L., Allègre, C.J., 1992. Clues to early solar system history from chromium isotopes in carbonaceous chondrites. Nature 358, 465–470.
Roth, A.S.G., Baur, H., Heber, V.S., Reusser, E., Wieler, R., 2009. Cosmic-ray-produced helium and neon in chondrules in Allende and Murchison. Lunar Planet. Sci. 40, 1838.
Rowe, M.W., Bogard, D.D., Brothers, C.E., Kuroda, P.K., 1965. Cosmic-ray-produced xenon in meteorites. Phys. Rev. Lett. 15, 843–845.
Rubin, A.E., Mittlefehldt, D.W., 1992. Classification of mafic clasts from mesosiderites: implications for endogenous igneous processes. Geochim. et Cosmochim. Acta 56, 827–840.
Russel, W.A., Papanastassiou, D.A., Tombrel, T.A., 1978. Ca isotope fractionation on the Earth and other solar system materials. Geochim. et Cosmochim. Acta 42, 1075–1090.
Schaeffer, O.A., Heymann, D., 1965. Comparison of CI–Ar and Ar–Ar cosmic ray exposure ages of dated fall iron meteorites. J. Geophys. Res. 70, 215–244.
Scherer, P., Schultz, L., 2000. Noble gas record, collisional history, and pairing of CV, CO, CK, and other carbonaceous chondrites. Meteor. Planet. Sci. 35, 145–153.
Scherer, P., Herrmann, S., Schultz, L., 1998. Noble gases in 21 Saharan LL-chondrites: exposure ages and possible pairings. Meteor. Planet. Sci. 33, 259–265.
Scherer, E.E., Cameron, K.L., Blichert-Toft, J., 2000. Lu–Hf garnet geochronology: closure temperature relative to the Sm–Nd system and the effects of trace mineral inclusions. Geochim. et Cosmochim. Acta 64, 3413–3432.

Scherer, E., Münker, C., Mezger, K., 2001. Calibration of the lutetium–hafnium clock. Science 293, 683–687.
Scherer, E.E., Mezger, K., Münker, C., 2003. The ^{176}Lu decay constant discrepancy: terrestrial samples vs. meteorites. Meteor. Planet. Sci. 38 (Suppl. A136).
Schlüter, J., Schultz, L., Thiedig, F., Al-Mahdi, B.O., Abu Aghreb, A.E., 2002. The Dar al Gani meteorite field (Libyan Sahara): geological setting, pairing of meteorites, and recovery density. Meteor. Planet. Sci. 37, 1079–1093.
Schönbächler, M., Lee, D.-C., Rehkämper, M., Halliday, A.N., Fehr, M., Hattendorf, B., Günther, D., 2003. Zirconium isotope evidence for incomplete admixing of r-process components in the solar nebula. Earth Planet. Sci. Lett. 216, 467–481.
Schultz, L., Weber, H.W., Franke, L., 2005. Rumuruti chondrites: noble gases, exposure ages, pairing, and parent body history. Meteor. Planet. Sci. 40, 557–571.
Schuth, S., Rohrbach, A., Münker, C., Ballhaus, C., Garbe-Schönberg, D., Qopoto, C., 2004. Geochemical constraints on the petrogenesis of arc picrites and basalts, New Georgia Group, Solomon Islands. Contrib. Mineral. Petrol. 148, 288–304.
Schuth, S., Münker, C., König, S., Qopoto, C., Basi, S., Garbe-Schönberg, D., Ballhaus, C., 2009. Petrogenesis of lavas along the Solomon Island Arc, SW Pacific: coupling of compositional variations and subduction zone geometry. J. Petrol. 50, 781–811.
Sneden, C., Cowan, J.J., Gallino, R., 2008. Neutron-capture elements in the early galaxy. Annu. Rev. Astron. Astrophys. 46, 241–288.
Söderlund, U., Patchett, P.J., Vervoort, J.D., Isachsen, C.E., 2004. The ^{176}Lu decay constant determined by Lu–Hf and U–Pb isotope systematics of Precambrian mafic intrusions. Earth Planet. Sci. Lett. 219, 311–324.
Sprung, P., Schuth, S., Münker, C., Hoke, L., 2007. Intraplate volcanism in New Zealand: the role of fossil plume material and variable lithospheric properties. Contrib. Mineral. Petrol. 153, 669–687.
Srinivasan, G., Whitehouse, M.J., Weber, I., Yamaguchi, A., 2007. The crystallization age of eucrite zircon. Science 317, 345–347.
Thrane, K., Connelly, J.N., Bizzarro, M., Borg, L.E., Ulfbeck, D., 2006. Lu–Hf systematics of the angrite SAH99555. Meteorit. Planet. Sci 41 (suppl., 5340).
Trinquier, A., Birck, J.-L., Allègre, C.J., 2007. Widespread ^{54}Cr heterogeneity in the inner solar system. Astrophys. J. 655, 1179–1185.
Trinquier, A., Elliott, T., Ulfbeck, D., Coath, C., Krot, A.N., Bizzarro, M., 2009. Origin of nucleosynthetic isotope heterogeneity in the solar protoplanetary disk. Science 324, 374–376.
Upadhyay, D., Mezger, K., 2008. Nucleosynthetic and neutron capture induced Sm isotope anomalies in chondrites. Lunar Planet. Sci. 39, 1262.
Vervoort, J.D., Patchett, P.J., Gehrels, G.E., Nutman, A.P., 1996. Constraints on early Earth differentiation from hafnium and neodymium isotopes. Nature 379, 624–627.
Vockenhuber, C., Dillmann, I., Heil, M., Käppeler, F., Winckler, N., Kutschera, W., Wallner, A., Bichler, M., Dababneh, S., Bisterzo, S., Gallino, R., 2007. Stellar (n, γ) cross sections of ^{174}Hf and radioactive ^{182}Hf. Phys. Rev. C 75, 015804.
Vockenhuber, C., Bichler, M., Wallner, A., Kutschera, W., Dillmann, I., Käppeler, F., 2008. Measurement of the thermal neutron capture cross section and the resonance integral of radioactive ^{182}Hf. Phys. Rev. C 77, 044608.
Weyer, S., Münker, C., Rehkämper, M., Mezger, K., 2002. Determination of ultra-low Nb, Ta, Zr and Hf concentrations and the chondritic Zr/Hf and Nb/Ta ratios by isotope dilution analyses with multiple collector ICP-MS. Chem. Geol. 187, 295–313.
Wisshak, K., Voss, F., Käppeler, F., Kazakov, L., Bečvář, F., Krtička, M., Gallino, R., Pignatari, M., 2006. Fast neutron capture on the Hf isotopes: cross sections, isomer production, and stellar aspects. Phys. Rev. C 73, 045807.
Wombacher, F., Rehkämper, M., Mezger, K., Bischoff, A., Münker, C., 2008. Cadmium stable isotope cosmochemistry. Geochim. et Cosmochim. Acta 72, 646–667.
Yin, Q., Jacobsen, S.B., Yamashita, K., 2002. Diverse supernova sources of pre-solar material inferred from molybdenum isotopes in meteorites. Nature 415, 881–883.
Yin, Q.-Z., Lee, C.-T.A., Ott, U., 2006. Signatures of the s-process in presolar silicon carbide grains: barium through hafnium. Astrophys. J. 647, 676–684.